SUPPLEMENTARY INFORMATION

Temperature-Jump Solution X-ray Scattering Reveals Distinct Motions in a Dynamic Enzyme

Michael C. Thompson[1], Benjamin A. Barad[1,2], Alexander M. Wolff[1,2], Hyun Sun Cho[3], Friedrich Schotte[3], Daniel M.C. Schwarz[1,4], Philip A. Anfinrud[3,#], James S. Fraser[1,*]

[1]Department of Bioengineering and Therapeutic Sciences, University of California, San Francisco, San Francisco, CA 94158, USA

[2]Biophysics Graduate Program, University of California, San Francisco, San Francisco, CA 94158, USA

[3]Laboratory of Chemical Physics, National Institute of Diabetes and Digestive and Kidney Diseases, National Institutes of Health, Bethesda, MD 220892-0520, USA

[4]Chemistry and Chemical Biology Graduate Program, University of California, San Francisco, San Francisco, CA 94158, USA

[#] - anfinrud@nih.gov

[*] - jfraser@fraserlab.com

Table of Contents

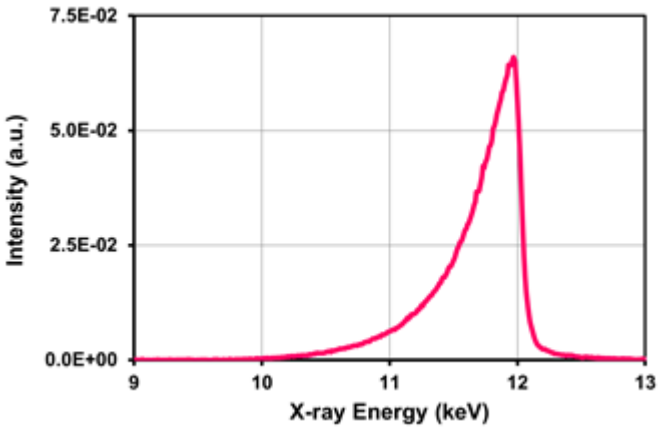

Supplementary Figure 1. Pink beam energy spectrum. Typical X-ray energy spectrum of the pink beam (3% energy bandwidth) used for the reported SAXS/WAXS measurements.

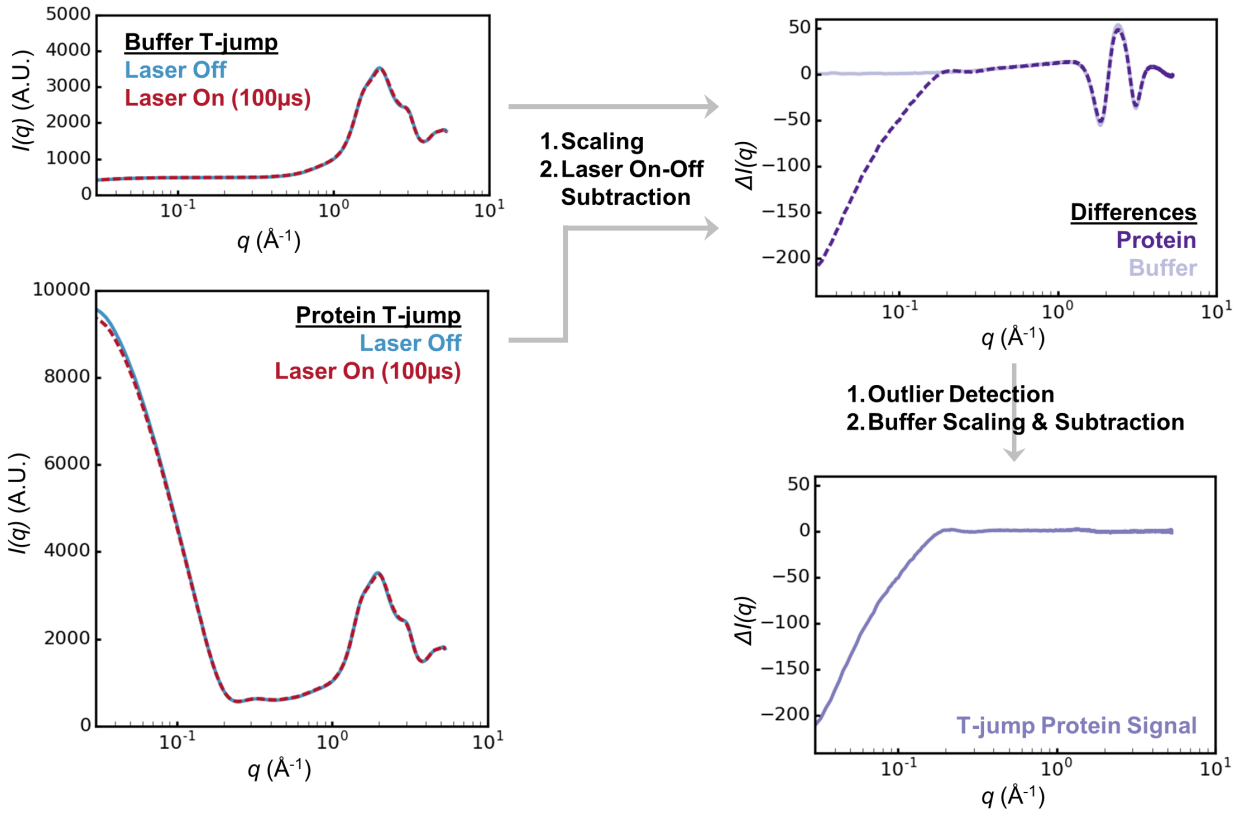

Supplementary Figure 2. Reduction of T-jump SAXS/WAXS data. T-jump data processing involves a combination of scaling and subtraction operations that produce time-resolved difference scattering curves. For each “laser on-off” pair, the recorded scattering curves are scaled to one another and the “laser off” curve is then subtracted from the “laser on” curve. This procedure is done independently for samples containing buffer only, and for protein samples. Next, the resulting difference curve for the buffer only sample is scaled to the difference curve obtained for the protein sample, and an additional buffer subtraction is performed to remove the thermal signal from the solvent. The result of this procedure is a difference scattering curve containing signal from the protein molecules only.

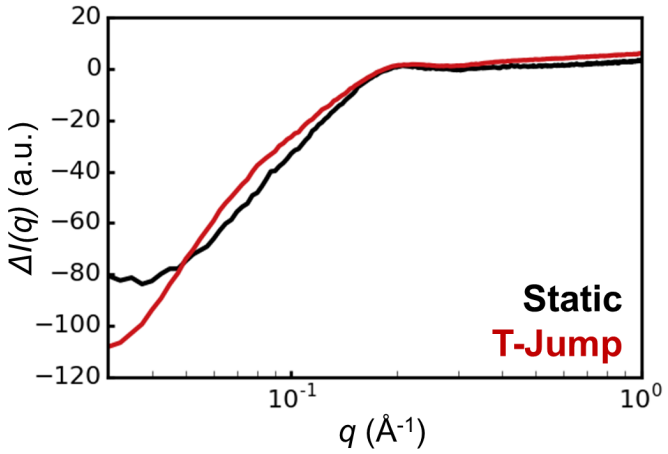

Supplementary Figure 3. Comparison of static and time-resolved differences. Static scattering differences between CypA solutions at 13°C and 23°C (black curve), and time resolved differences (100μs-laser off) for a T-jump spanning a temperature range of approximately 15°C and 26°C (red curve) are shown, demonstrating that the time-resolved signal equilibrates to approximately what would be expected based on static measurements.

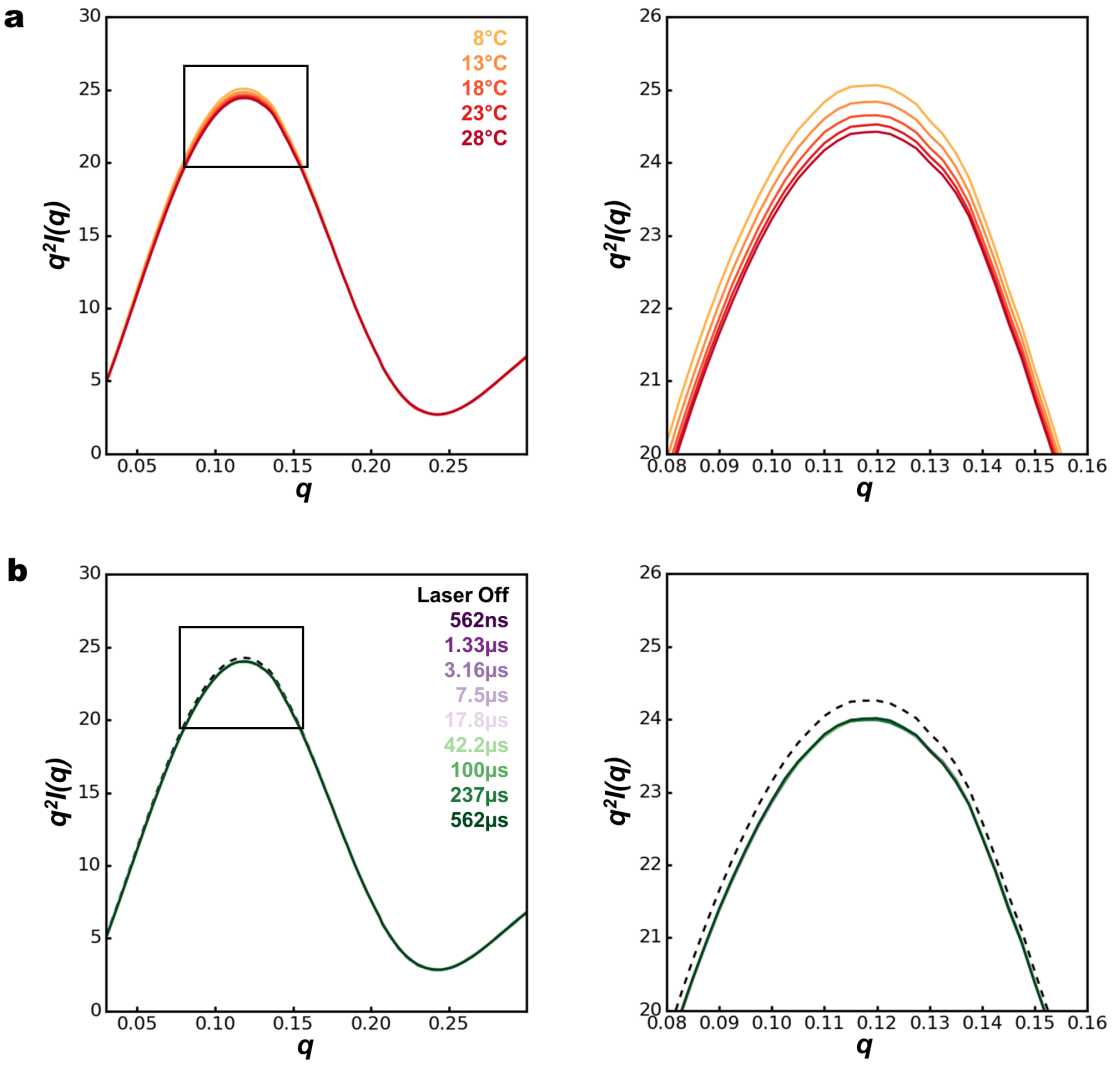

Supplementary Figure 4. Kratky plots for CypA reveal a small thermal disorder effect without protein unfolding. a) Kratky plots calculated as a function of static temperature, from 8°C to 28°C. The right panel shows an expanded view of the boxed region. **b)** Kratky plots calculated as a function of time delay for time-resolved T-jump data (colored lines, T-jump from approximately 15°C to 26°C). Again, the right panel shows an expanded view of the boxed region. All time delays show a similar difference relative to the "laser off" state (black dashed line), indicating that the underlying structural change is faster than the measurement dead time of our experiment.

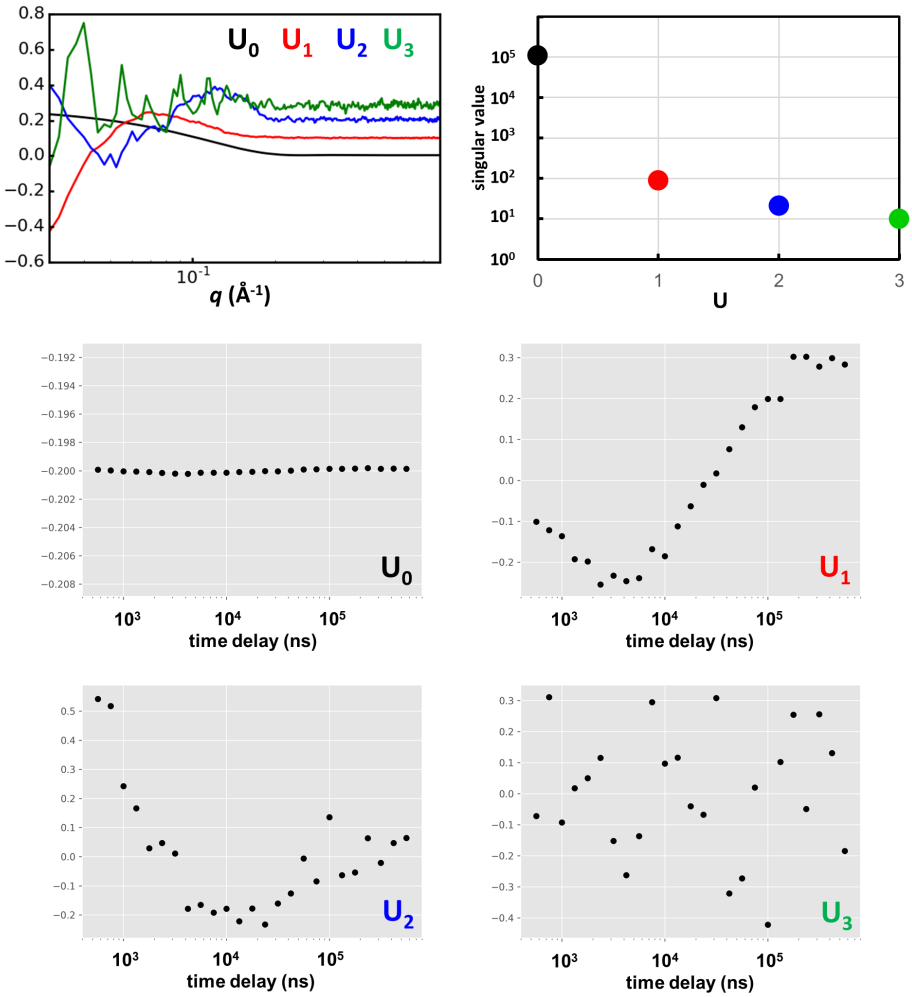

Supplementary Figure 5. Kinetic analysis of X-ray scattering by singular value decomposition (SVD). We used SAXS curves representing the time-resolved scattering at each time delay spanning 562ns and 562μs to construct a matrix, which was analyzed by SVD. The top left panel shows the top four left singular vectors ($\mathbf{U}_n$), and the top right panel shows their corresponding singular values. The lower panels are constructed from the right singular vectors, and show the time-dependent contribution of each left singular vector to the total signal. We note that the primary time-resolved signal is contained in just one singular vector ($\mathbf{U}_2$), whose time-dependent behavior reflects that of the integration analysis described in the main text.

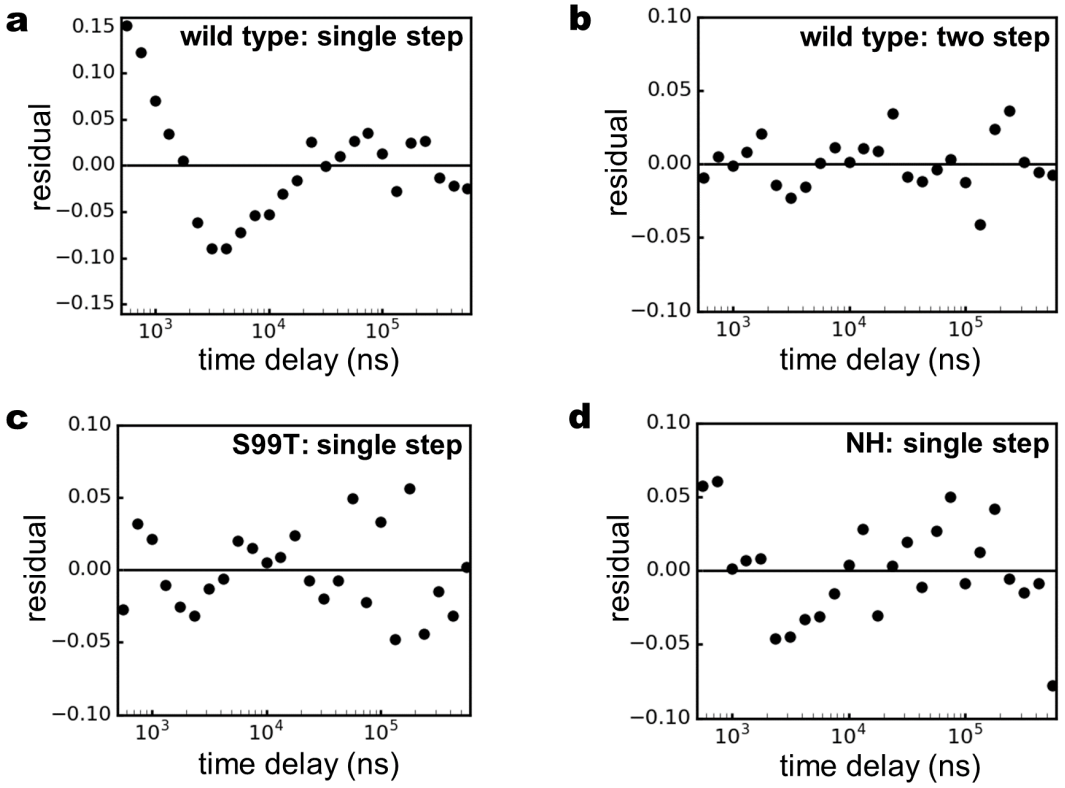

Supplementary Figure 6. Residuals for kinetic fits of T-jump SAXS/WAXS data for CypA variants. Residuals are shown for the following variants and fitting procedures: **a)** Wild type, single-step relaxation. **b)** Wild type, two-step relaxation. **c)** S99T mutant, single-step relaxation. **d)** NH double mutant, single-step relaxation. When the wild type data are modeled using a single kinetic step (**a**), the residuals show structure indicative of a second exponential process. In contrast, other fits show residuals with random fluctuations about zero (**b, c, d**), indicating an appropriate number of steps were included in the kinetic models.

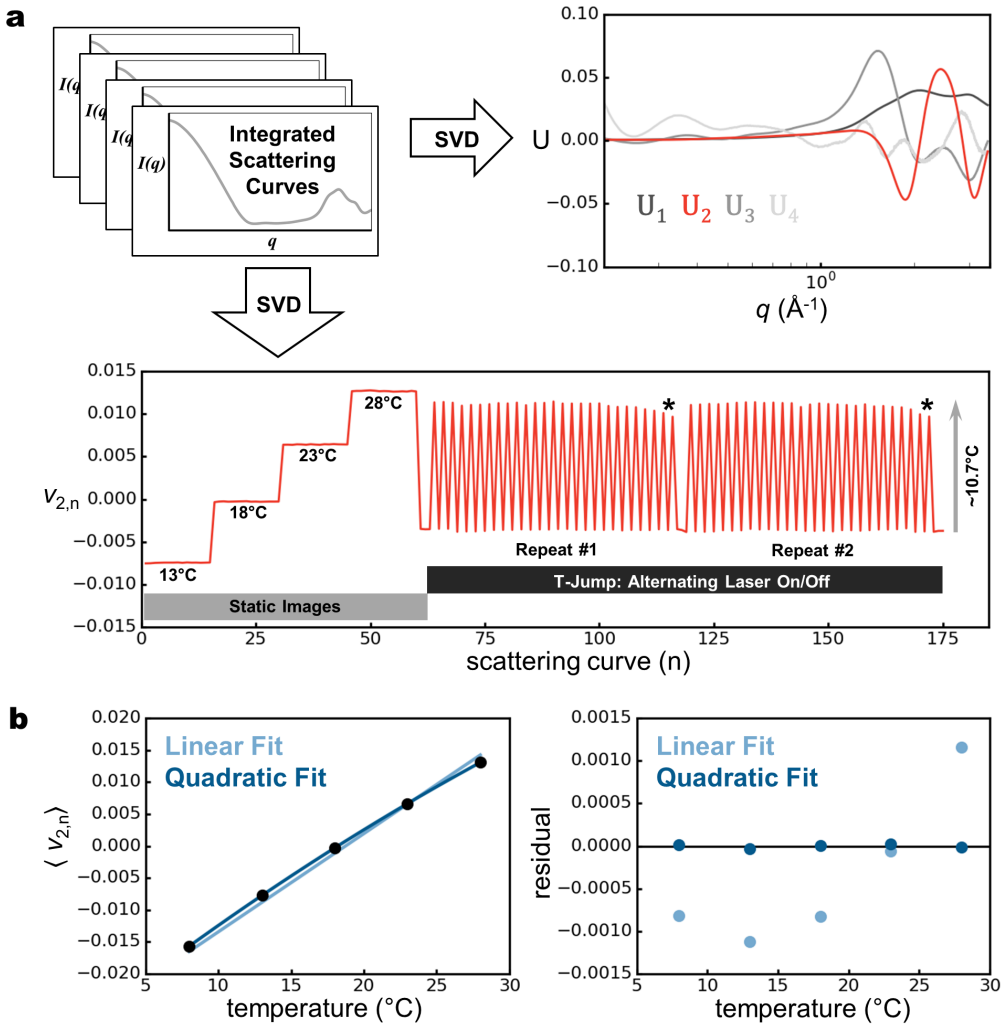

Supplementary Figure 7. X-ray scattering from bulk water acts as a sensitive thermometer for T-jump experiments. a) Using singular value decomposition (SVD), we can identify a signal whose contribution to each scattering curve is strongly dependent on the temperature. The left singular vectors with the four highest singular values are shown, with the vector corresponding to the temperature-dependent signal (U2) colored red. The contribution of this vector (v2,n) to each of 175 scattering curves is also shown. This set of 175 scattering curves includes static measurements (no pump laser) at four different temperatures, followed by two repeats of time-resolved T-jump measurements. The T-jump data were collected as "laser on-off" pairs, and within a single repeat each successive on-off pair was collected with an increasing pump-probe time delay. Cooling is evident at longer pump-probe time delays (denoted by *). **b)** To calculate the magnitude of the laser-induced T-jump, we used the static data to determine the average value of v2,n as a function of temperature, and fit the data using both linear and quadratic models. Based on the residuals for the two fits, we chose to use the resulting quadratic equation to determine the magnitude of the laser-induced T-jump using the values of v2,n calculated for the time-resolved scattering curves by SVD.

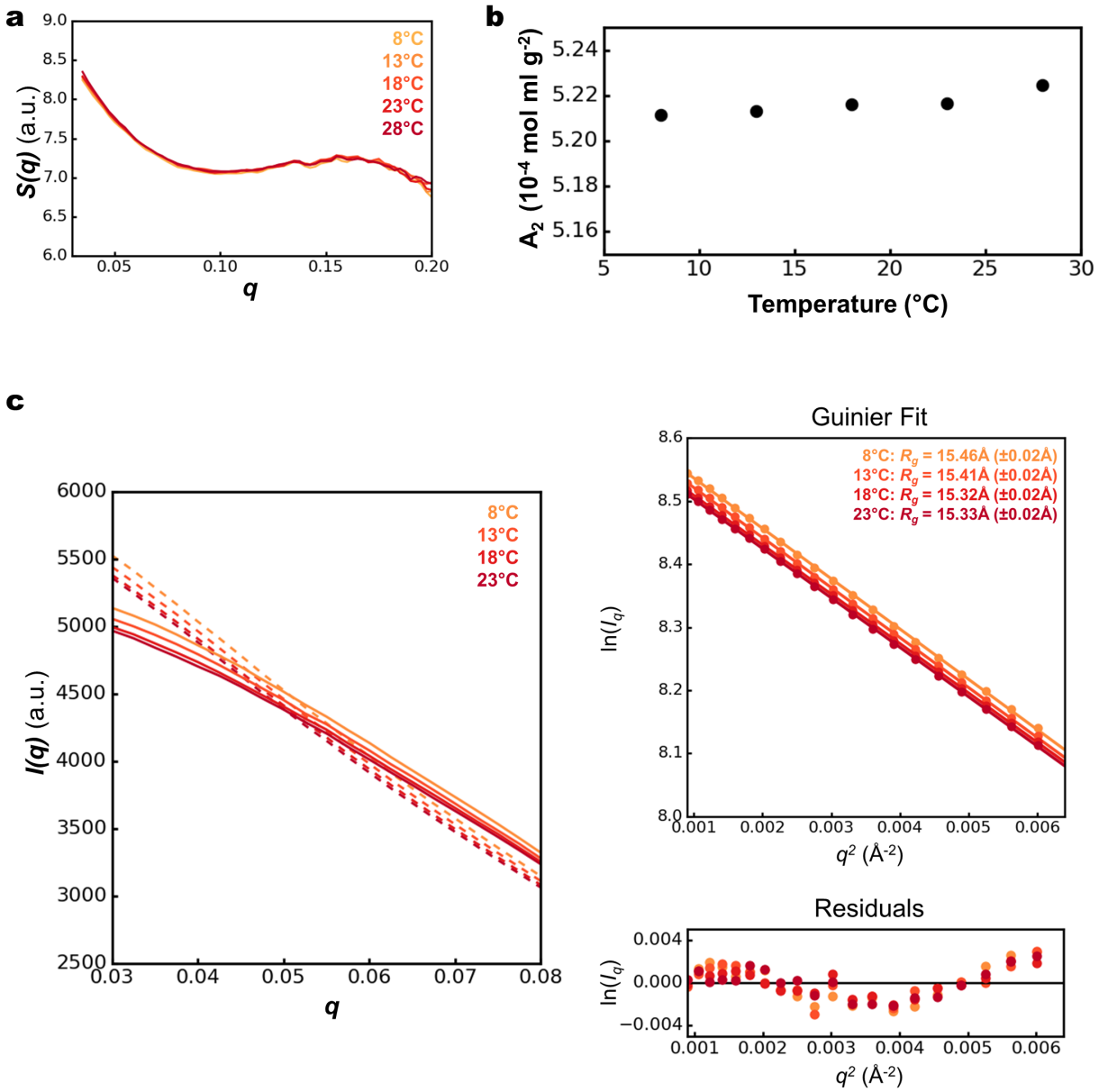

Supplementary Figure 8. Intermolecular interactions are not temperature dependent for CypA solutions. A) Both structure factors (S(q) in panel **a**) and second virial coefficients (A2 in panel **b**) calculated for 50mg/mL CypA solutions (wild type) are unchanged over temperatures ranging from 8-28°C. Low angle scattering is affected by interparticle interactions (dashed lines in panel **c**, left), however the effects can be removed by "infinite dilution extrapolation" (solid lines in panel **c**, left). Guinier analysis (panel **c**, right) using the curves that are corrected for interparticle interactions shows that these effects can be successfully removed, and that the radius-of-gyration can be accurately determined at different temperatures.

CypA Variant	Temperature (°C)	Temperature (K)	k_1 (10^4 s^{-1})	k_2 (10^4 s^{-1})
WT	6.2 ± 0.2	279.2 ± 0.2	N/A	1.1± 0.3
WT	11.4 ± 0.2	284.4 ± 0.2	43 ± 7	1.2 ± 0.2
WT	15.9 ± 0.2	288.9 ± 0.2	49 ± 10	2.5 ± 0.3
WT	17.0 ± 0.1	290.0 ± 0.1	58 ± 11	1.6 ± 0.2
WT	21.5 ± 0.1	294.5 ± 0.1	57 ± 7	2.2 ± 0.2
WT	23.8 ± 0.2	296.8 ± 0.2	117 ± 33	2.2 ± 0.2
WT	25.5 ± 0.2	298.5 ± 0.2	53 ± 33	2.7 ± 0.9
WT	26.7 ± 0.1	299.7 ± 0.1	98 ± 12	2.5 ± 0.2
WT	29.9 ± 0.1	302.9 ± 0.1	116 ± 24	2.4 ± 0.2
S99T	25.5 ± 0.2	298.5 ± 0.2	34 ± 4	N/A
D66N/R69H	27.1 ± 0.1	300.1 ± 0.1	N/A	4.1 ± 0.6

Supplementary Table 1. Calculated rates for the fast (k1) and slow (k2) relaxation processes measured from all T-jump experiments reported here. Note that kinetic analyses for the S99T and NH variants were performed at 25.5°C and 27.1°C respectively.

SUPPLEMENTARY DATA

Calibrating the Magnitude of the Temperature-Jump by Singular Value Decomposition

To characterize the temperature-dependent behavior of the solvent scattering, we performed static SAXS/WAXS measurements of our CypA samples as a function of temperature (equilibrium, no IR laser), in addition to our time-resolved measurements. We pooled these static, temperature-dependent SAXS/WAXS curves (azimuthally integrated *I(q)* v. *q*) with the time-resolved SAXS/WAXS curves from our T-jump measurements, and performed singular value decomposition (SVD) on a matrix constructed from the set of pooled curves (**Figure 7a**). Specifically, each column of this matrix represents a scattering curve, with each row of the matrix corresponding to a *q*-bin and the entries in the matrix corresponding to measured scattering intensities. The SVD analysis, which was performed over the q=0.07-3.45Å^{-1} region of the scattering curves, identified a signal (a left singular vector) whose prominent features were found in the *q*-region corresponding to the scattering of bulk water (q > 1.0) (**Figure 7a**). By extracting the entries in the corresponding row of the V matrix (containing the right singular vectors as columns), we could determine how this singular vector contributed to each scattering curve and demonstrate that its contribution was strongly temperature-dependent. Specifically, in the static (no T-jump) scattering curves the contribution of this singular vector increased with temperature, and for T-jump measurements the contribution of this vector to the observed scattering curves is perfectly correlated to the application of the pump laser pulse over sequential "laser on-off" pairs of X-ray measurements (**Figure 7a**), providing positive confirmation of a T-jump. Additionally, it is notable that the shape of the left singular vector used to monitor the temperature by SVD is nearly identical to that of the on-off difference signal at high-*q*.

The identification of a temperature-dependent singular vector provided a simple way to measure the magnitude of the laser-induced T-jump[1–5]. For each of the five static temperatures we explored, we calculated the average value of $v_{2,n}$, the entry in the matrix V that describes the contribution of the temperature-dependent singular vector (U_2) to the nth scattering curve, across 32 individual X-ray scattering curves. We then plotted the average $v_{2,n}$ vs. temperature and fit the data using both linear and quadratic models (**Figure 7b**). We examined the residuals for the two fits, determined the quadratic fit produced the most appropriate "standard curve" for estimation of the sample temperature from the SVD analysis, and used the resulting second-degree polynomial to estimate the temperature for each scattering curve in our series of time-resolved measurements. We compared the temperatures calculated for neighboring "laser on" and "laser" off scattering curves, and found the average T-jump produced by our IR heating pulse to be approximately 10.7°C. We observed that $v_{2,n}$ was consistent as a function of pump-probe time delay out to delay times of approximately 562μs, and decreased for longer time delays, implying that significant cooling of the sample occurred in less than 1 millisecond. Consequently, we limited our subsequent analysis to time delays shorter than 562μs.

Additional details about the temperature calibration are provided in the **Supplementary Methods** section.

Characterization of Interparticle Interactions and Structure Factor Corrections

Because the main time-resolved signal change was confined to very low-*q*, we wanted to ensure our time-resolved signal was due to a change in the protein's form factor (infinite dilution), and not the structure factor of the protein solution. This process was challenging due to low signal-to-noise at high-q, as well as our inability to measure very low-angle scattering using the available instrumentation. However, static measurements allowed us to identify the contribution of interparticle scattering, demonstrate that this contribution is invariant to temperature over the

range of our measurement conditions, and correct for its effect. To test whether changes in the radial distribution function originated from structural changes within the individual protein particles and their associated solvent and not from changes in the relative arrangement of the CypA molecules in solution, we performed static SAXS/WAXS measurements of CypA as a function of both temperature and CypA concentration. Using these data, we calculated the structure factor (*S(q)*) for a 50mg/mL CypA solution at multiple different temperatures (see **Supplementary Methods**), and determined there was no significant difference in the q=0.03-0.2 $Å^{-1}$ region of the scattering curves (**Figure 8**), consistent with other work on similarly-sized protein molecules in solution [6]. Next, we plotted the second virial coefficient for CypA as a function of temperature, and noticed that this quantity shows only a very small temperature dependence that cannot account for the observed time-resolved differences. In contrast to our results for CypA, Bonneté, et al. performed similar calculations of second virial coefficients for lysozyme solutions at similar temperatures and buffer conditions, and calculated temperature-dependent changes that were 50-fold larger (or more) than what we determined for CypA[6]. This analysis also allowed us to correct for the effects of interparticle interactions through a procedure which allows extrapolation of the observed concentration-dependent scattering to "infinite dilution" (see **Supplementary Methods**). In addition to the direct measurements of interparticle interactions provided by concentration-dependent scattering measurements, we also used Guinier analysis (linear fit of $ln[I(q)]$ vs. q^2, see **Supplementary Methods**) to assess whether the radial distribution function (structure factor) of CypA particles in solution changes significantly upon temperature perturbation. We analyzed scattering curves derived from both static temperature data and from time-resolved data, and observed that while Guinier fits of the T-jump measurements do have larger residuals than those for static data, the residuals do not change substantially as a function of either temperature (in static experiments) or time (in time-resolved experiments).

Rapid Loss of X-ray Scattering Contrast due to Thermal Expansion

We believe the largest contributor to the fast reduction in I(0) signal is thermal expansion, whose effect is twofold. First, thermal expansion of the system in general results in the expulsion of some scattering material (solvent containing CypA protein particles) from the X-ray beam path, which has a constant volume during the experiment. The volumetric thermal expansion coefficient of liquid water is approximately $2.1*10^{-4}/K$ [7], and the sample is 95% water by mass, so the amount of material in the X-ray beam path decreases by approximately 0.2% for our T-jumps, which were approximately 11°C. Second, protein thermal expansion coefficients are estimated to be larger than those of liquid water, so heating of the sample results in a reduction of scattering density (loss of contrast) because the decrease in the average electron density of the protein particles is greater than that of the solvent. Using CypA crystal structures determined over a temperature range spanning 260-310K[8], we determined the thermal expansion coefficient of CypA to be approximately $4.1*10^{-4}/K$. The thermal expansion coefficient we calculated for CypA is similar to that of met-Myoglobin, which was reported to be $3.5*10^{-4}/K$ by [9,10]. Using our calculated thermal expansion coefficient for CypA and its average electron density calculated from a crystal structure, along with the analogous properties for bulk water [7], we estimate that the I(0) change due to thermal expansion is approximately 2.6% for our T-jump experiments; however, this approximation likely overestimates the effect of thermal expansion on the scattering density of CypA particles, because we calculated the thermal expansion coefficient of the protein using a linear fit of volume versus temperature over a broad temperature range. In contrast, the thermal expansion coefficient likely has some temperature dependence and our analysis may overestimate thermal expansion in the relevant temperature regime.

SUPPLEMENTARY METHODS

Sample Preparation

CypA samples were prepared as described previously[8,11]. Briefly, the recombinant protein was expressed in *E. coli* BL21(DE3) cells and purified by liquid chromatography. Cells were lysed by sonication at pH=6.5, the lysate was clarified by high-speed centrifugation, and CypA was captured from the clarified lysate using a HiTrap-SP cation-exchange column (GE Healthcare). The protein was eluted using a sodium chloride gradient, and fractions containing CypA were pooled, and the pH was shifted to 7.5. The resulting solution was applied to a HiTrap-Q anion exchange column (GE Healthcare), and CypA was collected in the column flow-through. Finally, a polishing step was performed using a Superdex-75 gel filtration column (GE Healthcare). The protein was concentrated to 50mg/mL in buffer containing 20mM HEPES (4-(2-hydroxyethyl)-1-piperazine-ethanesulfonic acid) buffer at pH=7.5, 50mM sodium chloride, and 0.5mM TCEP (tris-hydroxyethylphosphine). CypA mutants (S99T and NH) were prepared following the same protocol used for the wild type protein. We note that while 50mg/mL is a relatively high protein concentration for in vitro experiments, this is much lower than the typical intracellular protein concentration (approximately 300mg/mL), and that CypA has been demonstrated to undergo its functional motions even in the crystalline environment[8,11]. For all X-ray measurements performed on buffer only without protein, the buffer was taken from the concentrator filtrate.

T-Jump SAXS/WAXS Data Collection and Processing

Time-resolved SAXS/WAXS measurements of CypA were performed on the BioCARS beamline at the Advanced Photon Source, while the storage ring was operating in hybrid mode. Temperature-jump data were acquired using the pump-probe method, as described recently by Cho. et al. [4]. Fast temperature-jump was performed on a CypA solution (50mg/mL) in a silica capillary using an Opolette 355 II (HE) optical parametric oscillator (OPOTEK), which produced a 7ns laser pulse with a peak wavelength of 1443nm. The pump laser energy was approximately 1mJ per pulse, and the beam was focused to an elliptical spot with dimensions of 400μm by 60μm (FWHM, gaussian beam profile), yielding a photon fluence of ~50mJ/mm^2 at the sample, which heated a 50mg/mL CypA solution in a capillary. A suitably delayed X-ray pulse of 494ns duration (eight septuplets in APS hybrid mode) with a peak X-ray energy of 12keV and 3% energy bandwidth (pink beam, **Figure 1**), was used to probe the sample following the introduction of the T-jump, and the X-ray scattering was recorded using a Rayonix MX340-HS CCD detector. In our experiments, the temporal resolution is limited to approximately 500ns by the duration of the X-ray pulse, which is substantially longer than the duration of the IR pulse. To speed data acquisition, we utilized a sample holder and data collection scheme recently reported by Cho, et al,[4] which combined fast translation along the capillary axis with slow sample circulation via a peristaltic pump. The fast translation of the capillary allowed us to rapidly accumulate X-ray scattering from 41 pump-probe measurements on a single detector image by translating the capillary to a fresh position between each pump-probe pair. The slow circulation of the sample allowed us to replenish the protein solution and limit the extent of X-ray radiation damage by spreading the X-ray dose over a relatively large volume during long data collection runs. Data were collected as pairs of alternating "laser on" and "laser off" X-ray images. The pump-probe time delay was systematically increased with each successive on/off pair of images. We measured pump-probe time delays spanning three logarithmic decades from 562ns to 1ms, at a time density of eight points per decade. A total of 50 replicate X-ray images were collected for each pump-probe time delay. It is important to note that time-resolved X-ray measurements referred to herein as “laser off,” were followed (10μs) by application of an IR pulse to the sample, as described by Cho, et al.[4], which prevented the introduction of a temperature offset created by

incomplete cooling in between “laser on” and “laser off” measurements. A temperature controller integrated into the sample holder allowed us to initiate the T-jump from different starting temperatures, and also allowed us to collect static temperature data. Static temperature images were collected in a manner similar to the time-resolved images, but without application of the pump laser pulse. Data collection protocols were identical for protein and buffer samples.

After acquiring the data we applied polarization, geometry, and detector non-uniformity corrections to the 2D X-ray images. The scattering intensities (photons/pixel) were binned and averaged as a function of the scattering vector magnitude (q), yielding isotropic scattering curves ($I(q)$ vs. q; $q = 4\pi \cdot \sin(\theta)/\lambda$, where 2θ is the scattering angle and λ is the X-ray wavelength) [4]. Next, for each data collection run, we carried out outlier detection by performing singular value decomposition (SVD) on a matrix constructed from our integrated scattering curves. In this SVD, the left singular vector with the largest singular value represents the global average of all the scattering curves used to construct the input matrix. We analyzed the right singular vectors from the SVD to determine which images were irregular. Specifically, we calculated the mean value of $v_{1,n}$, the entry in the matrix $\mathbf{V}$ that describes the contribution of the right singular vector with the largest singular value ($\mathbf{U}_1$) to the n^{th} scattering curve, across all the input X-ray scattering curves. Then, if the value of $v_{1,n}$ for any specific scattering was more than 2.5 standard deviations above or below the mean, that image was discarded. Our outlier detection procedure is implemented in a Python script called “SVD_Quarantine.py.” By inspecting the results of the SVD, we decided to remove the first 5 repeats from each data set, as well as some additional outliers that failed our statistical test. The same averaging and outlier detection method was used for both static and time-resolved measurements.

Scaling of X-ray Scattering Curves

All scaling of X-ray scattering curves was performed using an algebraic (least-squares) procedure. To determine the scale factor, A, which can be applied to a scattering curve $I(q)_a$ in order to scale it to a second scattering curve $I(q)_b$, we used the following equation:

$$A = \frac{\sum_q I(q)_a I(q)_b}{\sum_q I(q)_a^2} \qquad \text{Eq. 2}$$

Although we used the equation above for scaling throughout our analysis, the q-range to which it was applied varied depending on the context, and details are provided below.

X-ray Thermometry

Following the initial data processing steps described above, we used singular value decomposition (SVD) to determine the magnitude of the T-jump introduced by the IR laser pulse[1–5]. We pooled static, temperature-dependent SAXS/WAXS curves (azimuthally integrated $I(q)$ v. q) with the time-resolved SAXS/WAXS curves from time-resolved measurements, scaled them to a common reference over the q=0.025-4.28 Å^{-1} region, and performed SVD on a matrix built from these scaled curves. In this matrix, each column represents a single scattering curve, with the rows of the matrix corresponding to q-bins and the entries in the matrix consisting of azimuthally-averaged scattering intensities. The SVD analysis was performed using only the q=0.07-3.45 Å^{-1} region of the scattering curves. As described in the Results section, the SVD identified a left singular vector whose contribution to the overall scattering signal was highly temperature dependent. This was the left singular vector with the second largest singular value (U_2). For each of the five temperatures used for static data collection, we calculated the average value of $v_{2,n}$,

which is the entry in the matrix V describing the contribution of the temperature-dependent singular vector (U_2) to the n^{th} scattering curve. We then plotted the average $v_{2,n}$ vs. temperature and ultimately fit this data using a quadratic model. Finally, we used the resulting second-degree polynomial and the values $v_{2,n}$ for each time-resolved scattering curve to estimate the temperature for each T-jump measurement. By comparison of neighboring "laser on" and "laser off" scattering curves, we determined that the average T-jump was 10.7°C. Our thermometry procedure is implemented in a Python script called "thermometry_timepoints.py."

Data reduction: On-Off Subtraction, Repeat Averaging, and Buffer Subtraction

We implemented a data reduction procedure that operated on the integrated scattering curves generated using our data collection protocol and produced several outputs that were subsequently used for our kinetic and structural analyses. This procedure, implemented in a Python script called "reduce_data.py," took advantage of paired "laser on" and "laser off" measurements, redundant measurements of each pump-probe time-delay, and parallel T-jump experiments for samples containing protein and samples consisting of buffer only. The input for this script was essentially two data sets. The first, was a series of time-resolved scattering curves measured from a sample containing protein and consisting of paired "laser on/off" measurements with multiple replicate measurements of each pump-probe time delay (see above). The second was a similar data set, only collected from a sample containing buffer only and no protein. All of the input scattering curves were scaled to a common reference over the q=0.025-4.28Å^{-1} range, and "laser off" curves were subtracted from their associated "laser on" curves to create a difference scattering curve ($\Delta I(q)$) for each "laser on/off" pair. Next, all replicate difference curves (i.e. same sample and time delay) were grouped together, an iterative chi-squared test was performed (using a cutoff of χ^2=1.5), and the average difference curve was calculated for each pump-probe time delay in the series. For each time delay, the difference signal for the buffer only sample was scaled to the difference signal for the sample containing protein over the q=1.5-3.6 Å^{-1} range, and then the buffer signal was subtracted from the protein signal to isolate the difference signal due only to the protein. Additionally, this script took all of the "laser off" scattering curves, performed an iterative chi-squared test (cutoff of χ^2=1.5), and calculated their average. As was done for the difference curves, the average "laser off" scattering curve for buffer only was subtracted from the average "laser off" scattering curve for the protein sample after an additional scaling step (q=1.5-3.6 Å^{-1} range). The output of this data reduction procedure was a single scattering curve ($I(q)$ vs. q) for the "laser off" state, and a difference scattering curve ($\Delta I(q)$ vs. q) for each pump-probe time delay. All output data were corrected for the contribution of the buffer, and errors were propagated from the initial measurement standard deviations.

Kinetic Analysis

The averaged difference curves produced by our data reduction procedure were used for kinetic analysis of the time-resolved signal changes, which was implemented in a Python script called "difference_dat_kinetics.py." For each time delay, this script integrated the area under the difference curve over the q=0.03-0.05 Å^{-1} range, then fit the resulting data (integrated area vs. time) to calculate relaxation rates using non-linear least-squares curve fitting. We used the following equations, for single-step kinetic fits:

$$A\left(1 - e^{-k_1 t}\right) + B \qquad \text{Eq.3}$$

And for two-step kinetic fits:

$$A\left(1 - e^{-k_1 t}\right) + B\left(1 - e^{-k_2 t}\right) + C \qquad \text{Eq. 4}$$

The output of this analysis was a relaxation rate, or two rates, with standard deviations calculated using a bootstrapping method[12]. The use of a bootstrap procedure was deemed appropriate, because standard deviations calculated for the integrated area under the difference scattering curves are likely to overestimate the true error, as they are the result of propagating measurement standard deviations through radial integration, scaling, on-off subtraction, averaging, buffer subtraction, and difference curve integration, with all experimental errors assumed to be random. In contrast, some experimental error is likely systematic, and would instead be removed, rather than propagated, by the subtractive operations employed during data processing. In cases where we performed T-jumps at multiple temperatures, we used the observed rates and their standard deviations to perform an Eyring analysis by fitting Eq. 1 (above) using a least-squares method to determine the enthalpy and entropy of activation, and their standard deviations (using the covariance matrix). We implemented the Eyring analysis in a Python script called "eyring_fit.py."

Creation of High-Quality Time-Resolved Scattering Curves for Structural Analysis

To produce high-quality scattering curves that could be used for real space interpretation of the time-resolved X-ray scattering, we took the following steps. We used all of the "laser off" scattering curves from our on-off paired time-resolved measurements to create a single average curve. Then, for each of the time-delays reported, we added the average on-off difference (see above) to this average "laser off" scattering curve:

$$I(q)_t = \langle I(q)_{off} \rangle + \langle \Delta I(q)_t \rangle \qquad \text{Eq. 5}$$

Calculating the time-resolved scattering curves in this manner allows us to take advantage of the data collection structure, specifically the collection of "laser on and off" pairs, and many replicate measurements to remove some effects of systematic error that can accumulate during the course of long experiments and can mask small time-resolved differences in X-ray scattering. Next, we utilized static scattering measurements, as a function of both concentration and temperature, to characterize the effect of intermolecular interactions on the observed X-ray scattering and to calculate structure factors (*S(q)*) for our 50mg/mL CypA solutions at temperatures spanning a range relevant to our T-jump experiments. We calculated structure factors (and second virial coefficients) following the methods described by Bonneté, et al. [6]. The scattering curves derived from summing the average "laser off" signal and the time-resolved differences were then divided by the calculated structure factors to correct for intermolecular interactions and extrapolate our measurements to infinite dilution. Because we discovered that the effect of intermolecular interactions was not temperature dependent, we did not need to model the time-dependence of structure factors for our protein solutions following the T-jump, and the structure factor calculated at 13°C was used for the infinite dilution extrapolation. The calculation of structure factors and the creation of the high-quality, corrected *I(q)* curves were implemented in a pair of Python scripts called "structure_factor_calc.py" and "structure_factor_correction_TR.py," respectively (a script called "structure_factor_correction_static.py," was used in the latter step for static data sets).

Guinier Analysis and Calculation of R_g

In order to calculate radii-of-gyration (R_g) and to extrapolate the value of *I(0)* from scattering curves, we used the linear Guinier approximation:

$$ln[I(q)] = ln[I(0)] - \frac{R_g^2}{3} \cdot q^2$$ Eq. 6

Guinier analysis was performed over the q-region spanning 0.03-0.08Å^{-1}. We note that scattering curves were not placed on an absolute scale, however, this is not a requirement for Guinier analysis. The calculations were implemented in a Python script called “rg_and_i0.py.”

SUPPLEMENTARY REFERENCES

1. Cammarata, M. *et al.* Impulsive solvent heating probed by picosecond x-ray diffraction. *J. Chem. Phys.* **124**, 124504 (2006).
2. Kjær, K. S. *et al.* Introducing a standard method for experimental determination of the solvent response in laser pump, X-ray probe time-resolved wide-angle X-ray scattering experiments on systems in solution. *Phys. Chem. Chem. Phys.* **15**, 15003–15016 (2013).
3. Arnlund, D. *et al.* Visualizing a protein quake with time-resolved X-ray scattering at a free-electron laser. *Nat. Methods* **11**, 923–926 (2014).
4. Cho, H. S. *et al.* Dynamics of Quaternary Structure Transitions in R-State Carbonmonoxyhemoglobin are Unveiled in Time-Resolved X-ray Scattering Patterns Following a Temperature Jump. *J. Phys. Chem. B* (2018). doi:10.1021/acs.jpcb.8b07414
5. Rimmerman, D. *et al.* Direct Observation of Insulin Association Dynamics with Time-Resolved X-ray Scattering. *J. Phys. Chem. Lett.* **8**, 4413–4418 (2017).
6. Bonneté, F., Finet, S. & Tardieu, A. Second virial coefficient: variations with lysozyme crystallization conditions. *J. Cryst. Growth* **196**, 403–414 (1999).
7. Irvine, T. F. & Duignan, M. R. Isobaric thermal expansion coefficients for water over large temperature and pressure ranges. *Int. Commun. Heat Mass Transfer* **12**, 465–478 (1985).
8. Keedy, D. A. *et al.* Mapping the conformational landscape of a dynamic enzyme by multitemperature and XFEL crystallography. *Elife* **4**, (2015).
9. Frauenfelder, H. *et al.* Thermal expansion of a protein. *Biochemistry* **26**, 254–261 (1987).
10. Hiebl, M. & Maksymiw, R. Anomalous temperature dependence of the thermal expansion of proteins. *Biopolymers* **31**, 161–167 (1991).
11. Fraser, J. S. *et al.* Hidden alternative structures of proline isomerase essential for catalysis. *Nature* **462**, 669–673 (2009).
12. DiCiccio, T. J. & Efron, B. Bootstrap confidence intervals. *Stat. Sci.* 189–212 (1996).